Tailoring the Asymmetric Magnetoimpedance Response in Exchange-Biased Ni-Fe Multilayers

U. Kilic,[1] C. A. Ross,[2] and C. Garcia[3,*]

[1]*Department of Electrical and Computer Engineering, University of Nebraska-Lincoln, Lincoln, Nebraska 68588, USA*

[2]*Department of Materials Science and Engineering,Massachusetts Institute of Technology, Cambridge, Massachusetts 02139, USA*

[3]*Department of Physics, Universidad Técnica Federico Santa María, 2390123 Valparaíso, Chile*

The dependence of the asymmetric magnetoimpedance (MI) response on the directions of both the magnetic field and the exchange bias is studied for an [Ni-Fe(60 nm)/Ir-Mn(35 nm)] $\times$ 5 multilayer system. The antiferromagnetic (AFM) layers create an exchange bias that shifts both the hysteresis loop and the MI response of Ni-Fe; the strength of this coupling depends on the thicknesses of both the ferromagnetic layer and the AFM layer. Tuning the exchange-bias angle and the applied-magnetic-field direction provides a practical method to control the symmetry and the magnitude of the MI response. The observed asymmetric response can be attributed to the coexistence of two anisotropies, the induced exchange-bias anisotropy and the magnetocrystalline anisotropy. Both are distinct components of the exchange-coupled Stoner-Wohlfarth energy density that forms a basis for simulations within the conventional Landau-Lifshitz-Gilbert framework. The model reproduces the main features of the experimental results, providing a deeper understanding of the effect of the anisotropy components on the MI characteristic curve and ratio. The results can be used for the development of an asymmetric MI exchange-biased thin-film element in an autobiased linear-magnetic-field sensor.

I. INTRODUCTION

The magnetoimpedance (MI) effect consists of a significant change in the impedance of a magnetically soft conductor on the application of an external magnetic field. The MI effect requires a material with low magnetic anisotropy and high magnetic permeability. Since its discovery in 1994 [1,2], it has been a subject of great interest and has been widely studied in different systems, including wires [3], ribbons [4], films [5], and rolled-up tubes [6]. The remarkable linearity and sensitivity to small magnetic fields down to the picotesla regime make the MI effect very attractive in developing high-performance micromagnetic sensors for localized weak magnetic fields, such as in biomedical, automotive, space, and industrial applications.

The MI characteristic curve typically has two symmetric sharp peaks near the anisotropy field and shows nonlinear behavior around zero field. Such nonlinear characteristics could lead to serious problems if used for sensor applications when the operation occurs about the zero-magnetic-field point. Linearization is generally performed by application of a dc bias field or an electric current to the sensing element to obtain asymmetric characteristics,

but this is disadvantageous for many practical applications due to the energy consumption and the size of the bias electromagnet. Instead, establishing an asymmetric magnetic configuration helps to increase linearity and reduce the required dc bias [7].

Establishing an asymmetric MI (AMI) response has been achieved by two different approaches: static AMI due to asymmetry in the dc configuration [8,9] and dynamic AMI due to the mixing of the diagonal and off-diagonal components of the impedance tensor [9]. The second method, although not requiring additional power consumption, is inconvenient since it uses a coil in series with the MI element. Following the first approach, several methods have been developed to create asymmetry in MI behavior based on exchange bias (EB) in multilayer MI materials [10–14].

The use of EB in films is particularly attractive, since symmetric MI curves can be shifted along the applied magnetic field axis as reported for a Ni_{81}-Fe_{19}/Fe_{50}-Mn_{50} exchange-biased multilayer and in Ni_{81}-Fe_{19}/Ir-Mn, where the linear response can be easily shifted to zero field by change of the ac probe frequency [11,12].

In this article, we show how the asymmetric behavior in the shifted MI response of the MI peaks and the linear region of the MI curve of Ni-Fe/Ir-Mn multilayers can

———————
*carlos.garcia@usm.cl

be tailored by modification of the direction of both the exchange bias and the applied magnetic field. In addition, this linear response can be tuned with the frequency of the current.

Moreover, we develop a mathematical model for the magnetization reversal and MI field dependence of exchange-biased ferromagnetic thin films, from which the main characteristics of the thin-film magnetic behavior can be extracted, and compare it with the experimental results, obtaining excellent agreement. This model extends existing results by making available the full rotation of both the external magnetic field and the EB field for different anisotropy orientations. In addition, it also includes the contribution of the magnetoelastic energy, which, we find, affects the asymmetric response of exchange-biased systems. Our model generalizes the physics behind the giant-MI (GMI) effect in complex multilayer structures and provides full agreement with the experimental studies performed in an exchange-biased system. In summary, the system described here allows control over multiple variables that affect the asymmetric MI response and presents a comparison of experimental and model results taking into account the detailed definition of the effective magnetic field. These results will be useful in designing the linear response and the asymmetry of autobiased MI sensors.

II. EXPERIMENTAL PROCEDURE

Rectangular pieces of 3×12 mm^2 silicon wafers thermally oxidized with 50-nm SiO$_2$ are used as a substrate. Multilayer films of composition [Ni-Fe(60 nm)/ Ir-Mn(35 nm)] $\times$ 5 on 10-nm Ti, where Ni-Fe represents Ni$_{80}$-Fe$_{20}$, are deposited at room temperature by means of dc triode sputtering with a base pressure of 5.0×10^{-9} Torr and a deposition pressure of 1.0 mTorr. The thick multilayer structure and the number of repetitions are chosen to increase the MI response compared with that of a bilayer. The Ti(10 nm) underlayer is used to improve adhesion. XRD measurements confirm the growth of the antiferromagnetic (111) γ-fcc Ir-Mn phase on 5 nm of a highly textured (111) fcc Ni-Fe seed layer. A constant magnetic field of 250 Oe is applied in the sample plane during deposition to induce a magnetic exchange bias. The angle, ϕ_{EB}, between the long axis of the rectangular sample and the direction of the induced exchange-bias field H_{EB} is roughly $0°$ in sample 1, $45°$ in sample 2, and $90°$ in sample 3.

The static magnetization properties of the stripes are studied at room temperature by measurement of the hysteresis loops in a vibrating-sample magnetometer for different in-plane directions. The angle ϕ_{ext} between the applied magnetic field and the long axis is varied from $0°$ to $360°$ in steps of $15°$. Impedance, Z, is measured with a Hewlett-Packard network analyzer (model 8753C) with 0-dBm (1-mW) constant power following standard procedures [15].

III. THEORETICAL MODEL

To describe AMI phenomena, we develop a robust dynamic model that is governed by the conventional Landau-Lifshitz-Gilbert (LLG) equation of motion [16–18], written as follows:

$$\frac{\partial \mathbf{M}}{dt} = \underbrace{-\gamma \left(\mathbf{M} \times \mathbf{H}_{\text{eff}} \right)}_{\substack{\text{Precessional} \\ \text{torque}}} + \underbrace{\frac{\alpha}{M_s} \left(\mathbf{M} \times \frac{d\mathbf{M}}{dt} \right)}_{\substack{\text{Damping} \\ \text{torque}}}, \quad (1)$$

where $\mathbf{M}$ is the magnetization vector, γ is the gyromagnetic ratio, α is the Gilbert damping constant, and M_s is the saturation magnetization. The proposed framework based on this well-known equation is able to unravel the underlying mechanism of AMI phenomena by careful design of the effective magnetic field ($\mathbf{H}_{\text{eff}}$), which is given as follows:

$$\mathbf{H}_{\text{eff}} = \mathbf{H}_{\text{ext}} + \mathbf{H}_{\text{an}} + \mathbf{H}_{\text{EB}} + \mathbf{H}_D + \mathbf{H}_{\text{str}} + \mathbf{h}_{\text{alt}}(t), \quad (2)$$

where $\mathbf{H}_{\text{ext}}$ is the applied magnetic field (Zeeman field), $\mathbf{H}_{\text{an}}$ is the uniaxial-anisotropy field, $\mathbf{H}_{\text{EB}}$ is the exchange-bias field, $\mathbf{H}_D$ is the demagnetizing field [19,20], and $\mathbf{h}_{\text{alt}}(t)$ is the applied alternating magnetic field. The existence of a static magnetic field during the thin-film fabrication process creates a nonlinear Joule magnetostriction, and thus stores magnetoelastic energy, which is represented as $\mathbf{H}_{\text{str}}$ [17,21]. Inclusion of this contribution in the model brings about a more realistic approach to (A)GMI effects. As represented in the schematic illustration in Fig. 1, the inclusion of both ϕ_{ext} and ϕ_{EB} enables the external magnetic field and the exchange-bias field to rotate in the plane of the thin film. This simple but significant modification provides a powerful tool to model complex anisotropic systems such as the ones studied experimentally. The system magnetization can be written as follows:

$$\mathbf{M}_{\text{system}} = M_S \hat{z}' + \mathbf{m}_{\text{ac}} e^{j(wt)}, \quad (3)$$

where $\mathbf{m}_{\text{ac}}$ is a perturbation to the magnetization due to the presence of $\mathbf{h}_{\text{alt}}(t)$. For simplicity, the theoretical calculations are performed in the laboratory coordinate system $(\hat{x}', \hat{y}', \hat{z}')$ as shown in Eq. (3). Figure 1 shows the rotation of stationary coordinate axes $(\hat{x}, \hat{y}, \hat{z})$ to laboratory coordinate axes $(\hat{x}', \hat{y}', \hat{z}')$. It is worth noting that the magnetic domain configuration shown in Fig. 1 is just a particular case of the possible orientations of the magnetic moments. Figure 2 shows the generalized direction of magnetic domains that are used in the derivation of the resulting effective permeability and thus of the magnetoimpedance. Depending on the angle ψ (i.e., anisotropy orientation), a longitudinal magnetic moment orientation (i.e., all magnetic domains are aligned along the long axis) can also be obtained.
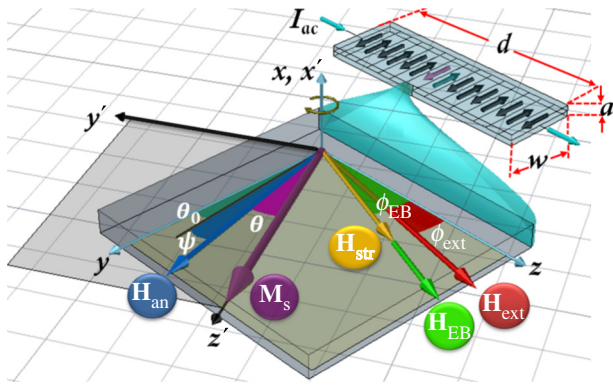
FIG. 1. The angles of the dc applied magnetic field, the ac magnetic field generated by the ac, and the exchange-bias field induced in the sample. The coordinate system is rotated from (x, y, z) to (x', y', z') for simplification of the theoretical calculations. The transverse magnetic domain configuration shown is just an example of possible domain orientations.

As reported in previous studies, for systems with transverse anisotropy, each magnetic domain has its own average magnetic moment alignment and permeability (μ_1 and μ_2) [16,17]. The system permeability tensor is regarded as the geometrical sum of both permeability components:

$$\mu_{\text{system}} = \frac{\mu_1 + \mu_2}{2}$$
$$= \begin{pmatrix} 1 + \chi & -j\,(\chi_a \sin(\theta)) & 0 \\ j\,(\chi_a \sin(\theta)) & \chi\,(\sin(\theta))^2 & 0 \\ 0 & 0 & 1 + \chi\,(\cos(\theta))^2 \end{pmatrix},$$

where χ and χ_a are the on-diagonal and off-diagonal susceptibility-tensor elements, respectively. This equation is obtained after the conversion of the coordinate system back to the stationary frame $(\hat{x}, \hat{y}, \hat{z})$. The tensor form of the system permeability (μ_{sys}) is the key to extract the effective permeability so as to obtain the MI response for a particular thin-film structure. The effective permeability is given by [22]

$$\mu_{\text{eff}} = 1 + \chi\,[\sin(\theta + \theta_0 + \psi)]^2 + \frac{\chi_a[\sin(\theta + \theta_0 + \psi)]^2}{1 + \chi}, \tag{4}$$

where θ_0 is a small angle between the transverse axis and the easy-axis direction. The angle ψ is postulated as an angle additional to θ_0 to enable the full rotation of the system in the anisotropy plane, and therefore the easy-axis orientation. Importantly, the angle θ is obtained from energy minimization ($\partial E_{\text{tot}}/\partial\theta = 0$). This calculation results in the determination of the easy axis for individual saturation-magnetization and in-plane-anisotropy orientations. The angle between saturation magnetization and the easy axis can be regarded as another dynamic input for the LLG
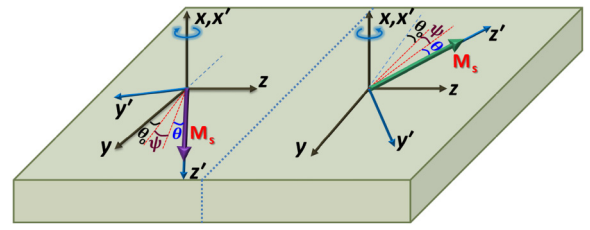

FIG. 2. Detailed schematic illustration of general magnetization-vector orientations in magnetic domains together with the angles: ψ is the angle between the main anisotropy axis and the magnetization vector, θ is the angle that minimizes the energy, and θ_0 is a small perturbation of the magnetization vector away from the transverse axis.

equation, the value of which changes when the external magnetic field is swept. Following this calculation, the MI response can be calculated by means of the following relation [16–18]:

$$Z = \frac{-\oint e \times h^* dS}{I_0^2} = R_{\text{dc}} \left(\frac{ka}{2}\right) \coth\left(\frac{ka}{2}\right), \tag{5}$$

where Z is the impedance of the material, h^* is the complex conjugate of the perturbed magnetic field, $k = \sqrt{2j/\delta}$, and a, δ, and R_{dc} are the thickness, skin depth, and dc resistance of the thin film, respectively.

The model incorporates the in-plane orientation of both the applied magnetic field and the exchange bias, in contrast with previously developed models [16–18].

IV. RESULTS AND DISCUSSION

Characteristic normalized hysteresis loops, measured at different applied-magnetic-field angles ϕ_{ext}, are presented in Fig. 3 from samples 1, 2, and 3, in which the exchange coupling makes an angle ϕ_{EB} of $0°$, $45°$, and $90°$, respectively, with the long geometrical axis. The dependence of measured exchange bias on the angle of the applied field during the hysteresis measurement is shown in Figs. 3(d)–(f). In each sample, H_{EB} reaches a maximum when $\phi_{\text{ext}} = \phi_{\text{EB}}$ and is zero in the normal direction. When $\phi_{\text{EB}} = 0°$ [Fig. 3(d)], H_{EB} reaches 34 Oe for $\phi_{\text{ext}} = 0°$ and $180°$, and for $\phi_{\text{ext}} = 45°$, $H_{\text{EB}} = 24$ Oe according to the expression $H_{\text{EB}}(\phi_{\text{ext}}) = H_{\text{EB}}(0°) \cdot \cos(\phi_{\text{ext}})$.

The static magnetic properties are known to affect the MI response [10,11]. Thus, in an exchange-biased sample, the MI and hysteresis curves are both shifted over the whole range of frequencies by an equal amount to the exchange-bias field. When the ferromagnetic layer thickness decreases, the exchange bias increases [12]. The impedance evolves from a single-peaked curve to a double-peaked curve as the frequency increases and the MI peak shifts to higher magnetic fields. [10,11]. The origin of this shift is attributed to the skin-depth variation from the frequency-dependent permeability of the Ni-Fe layer combined with the exchange-bias field.
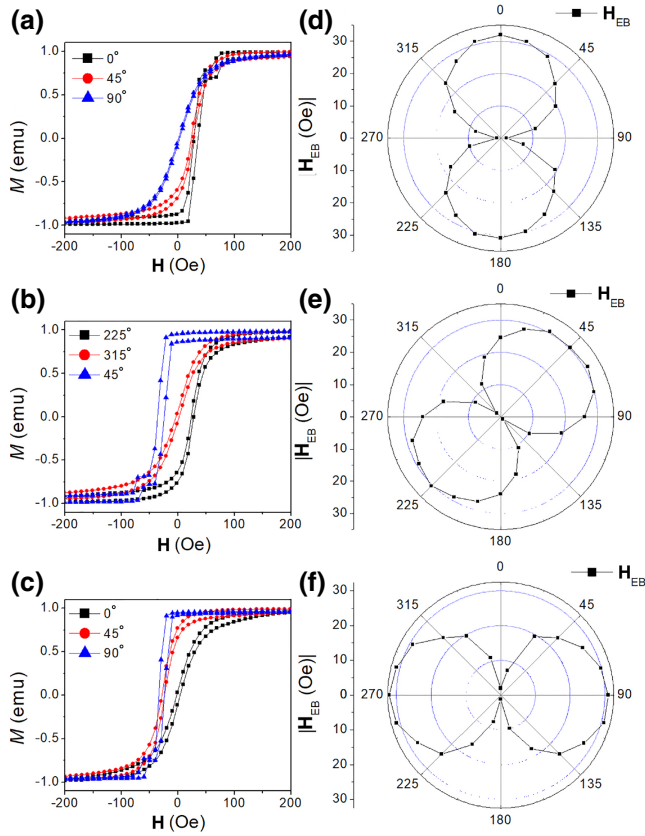
FIG. 3.   Hysteretic magnetization curves with an exchange-bias angle of (a) 0°, (b) 45°, and (c) 90° with respect to the sample long axis, measured at different applied-magnetic-field angles. (d)–(f) Dependence of the measured exchange bias on the applied magnetic field when the exchange bias makes an angle of (d) 0°, (e) 45°, and (f) 90° with the long axis.

FIG. 4.   Impedance ratio versus magnetic field for $\phi_{EB} = 0°$ at different angles between the applied magnetic field and the long axis: (a) $\phi_{ext} = 0°$, (b) $\phi_{ext} = 30°$, (c) $\phi_{ext} = 45°$, and (d) $\phi_{ext} = 90°$ measured at different applied-magnetic-field angles. (e) Modeling results.

Figure 4 shows the impedance ratio versus magnetic field curves of sample 1 ($\phi_{EB} = 0°$) at 1500 MHz measured at different magnetic field angles ($\phi_{ext} = 0°, 30°, 45°,$ and 90°). In this context, Z is defined as $Z = \sqrt{Z_{Re}^2 + Z_{Im}^2}$. When $\mathbf{H}_{ext}$ is parallel to $\mathbf{H}_{EB}$, the well-known symmetric MI response centered at $\mathbf{H}_{EB}$ [10,11] is observed. An increase in frequency shifts the peak position to higher magnetic fields. At 1500 MHz the asymmetry between the two peaks increases with the angle of the applied magnetic field. For $\phi_{ext} = 30°$ a noticeable asymmetric MI effect is present. The asymmetric behavior shows two characteristic features: (i) a shift of the MI-versus-field curve by an amount given by $H_{EB}(\phi_{ext}) = H_{EB}(0°) \cdot \cos(\phi_{ext})$ and (ii) asymmetry in shape given by the amplitude difference between the two peaks. For angles of 45° to less than 90°, the asymmetric double peak becomes a shifted asymmetric single peak (not shown). Figure 4(d) shows a MI response for $\phi_{ext} = 90°$ given by a wider, nonshifted symmetric single peak. MI curves measured from 90° to 360° exhibit a similar behavior. For angles larger than 90°, the single
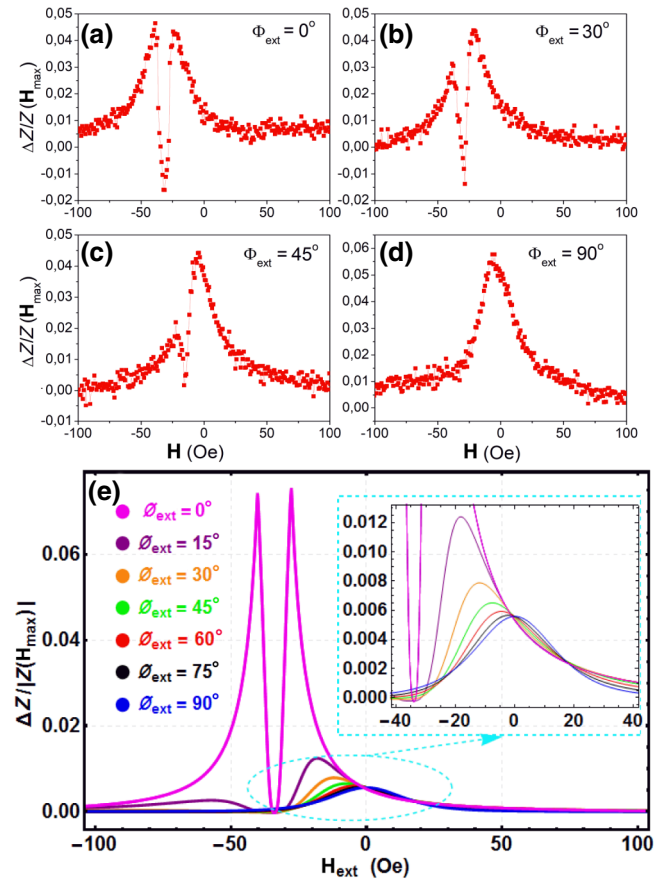
broad peak becomes progressively asymmetric and splits into two asymmetric peaks, and there is an increasing positive shift up to a maximum of 34 Oe at 180°. At 180° a symmetric two-peak behavior, similar to the one at 0°, is once again observed. A decrease in the MI magnitude occurs with an increase in the angle ϕ_{ext} between H_{EB} and H_{ext}.

The in-plane MI response of the thin film is expected to be slightly influenced by demagnetizing effects. This is attributed to the fact that the film thickness plays an essential role not merely in the out-of-plane demagnetizing factor ($N_x = 0.996$) but also in both the long-axis and the short-axis in-plane demagnetizing factors ($N_z = 2.95 \times 10^{-5}$ and $N_y = 4.3 \times 10^{-3}$, respectively).

Figure 5 shows data equivalent to the data in Fig. 4 but for sample 2, where $\phi_{EB} = 45°$. The coexistence of two different anisotropies leads to a complex MI behavior. When $\phi_{ext} = 45°$ or 225° [Fig. 5(a)], a symmetric MI response, shifted by 34 Oe, is observed. With increase of ϕ_{ext}, the two peaks become asymmetric and slowly shift toward zero field according to $H_{EB}(\phi_{ext}) = H_{EB}(0°) \cdot$
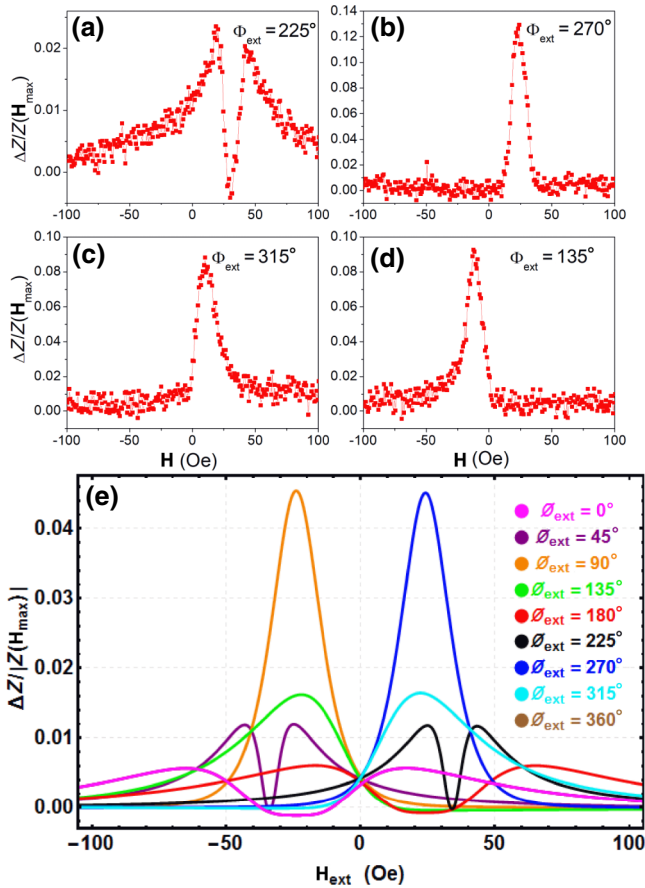
FIG. 5. Impedance ratio versus magnetic field for $\phi_{EB} = 45°$ at different angles of the applied magnetic field: (a) 225°, (b) 270°, (c) 315°, and (d) 135° with respect to the long axis. (e) Modeling results.

$\cos(\phi_{ext})$. At $\phi_{ext} = 90°$ or $-90°$ [Fig. 5(b)] a symmetric shifted MI curve is found. Finally, at $\phi_{ext} = 315°$ [Fig. 5(c)] or 135° [Fig. 5(d)] an asymmetric nonshifted MI behavior is observed. In the presence of exchange bias, the MI response varies depending on the magnitude of the longitudinal and transverse components of H_{ext}, due to its effect on the diagonal and off-diagonal susceptibility components. The alignment of magnetic moments along the easy axis is enhanced by the external magnetic field $\mathbf{H}_{ext}$, causing a double-peak MI response. Similar to the behavior of the MI response for sample 2, for the case of sample 3 with $\phi_{EB} = 90°$, the MI response preserves its astroid shape but it is rotated due to the energy contribution of H_{EB}. This exchange-bias energy further promotes transverse magnetization; therefore, the MI response is maximized at external-field orientations of $45° + n\pi/2$ (i.e., the midpoint between the long geometrical axis and the bias-field direction) where $n = 0, 1, 2,$ and 3. On the other hand, the minimum MI response corresponds to the orientations where the sample has the minimum susceptibility and response to H_{ext}. This occurs when $\mathbf{H}_{ext}$

is oriented at $n\pi/2$, where $n = 0, 1, 2,$ and 3. At these angles, H_{ext} requires more energy to perturb the spin system, which reduces the susceptibility. When $\phi_{ext} = 0°$, we observe a symmetric MI behavior centered at $H_{ext} = 0$. For increasing magnetic field angles, the MI curve shifts and the asymmetry of the two peaks increases, along with a reduction of the MI magnitude.

The model results are shown in Figs. 4(e) and 5(e). The simulations use $H_{EB} = 34$ Oe, $M_S = 790$ emu/cm^3, gyromagnetic ratio $\gamma_G = 2\pi(3.03)$ rad MHz/Oe, and $\alpha = 0.01$. K_{uni}, which represents the in-plane anisotropy, is varied between 1500 and 3200 erg/cm^3, but the model produces similar results over this range.

The direction of the uniaxial easy axis will be affected by the application of an external magnetic field during the deposition, and we assume the uniaxial easy axis is close to the direction of the induced exchange-bias field. However, the weak shape anisotropy will perturb the uniaxial-anisotropy direction. The field-annealing effect is taken into account as a contribution with the form of a magnetoelastic energy. Although this additional energy was noted in previous studies as a weak coupling effect, we see that it also plays a role in the orientation of the easy axis and therefore the uniaxial anisotropy, and has a contribution to the asymmetric response of exchange-biased systems. The value of the magnetoelastic energy will depend on the orientation of the applied magnetic field.

The experimental and modeling results agree well, but observed differences could be due to (i) a difference in the distribution of the easy axis, (ii) our disregarding the effect of exchange interactions on the MI response since the model accounts only for coherent rotation of the spins, and (iii) our modeling the system as a uniform thin-film layer instead of a multilayer stack, which might affect the easy-axis direction and therefore the evolution of the average magnetization vector.

To further understand the effect of the external-magnetic-field orientation on the MI response, the dependence of the MI ratio on the applied-magnetic-field angle ($\Delta Z/R_{DC}$ versus ϕ_{ext}) is extracted from MI versus H_{ext} plots. Each point of the plot corresponds to the maximum value of the MI curve measured for a given direction of the external magnetic field.

The outputs are shown in Fig. 6 for different exchange-bias angles ($\phi_{EB} = 0°$, 45°, and 90°) obtained from the model and are compared with experimental data for $\phi_{EB} = 45°$.

Figure 6 provides a way of visualizing the nonlinear behavior of the normalized MI ratio under full rotation of the external field for different exchange-bias orientations. The essential physics underlying Fig. 6 originates from how the spin system dissipates the Zeeman energy of the external magnetic field in the presence of exchange bias. The nonlinear trend of the MI response is dominated by the exchange bias, particularly the exchange-bias direction.
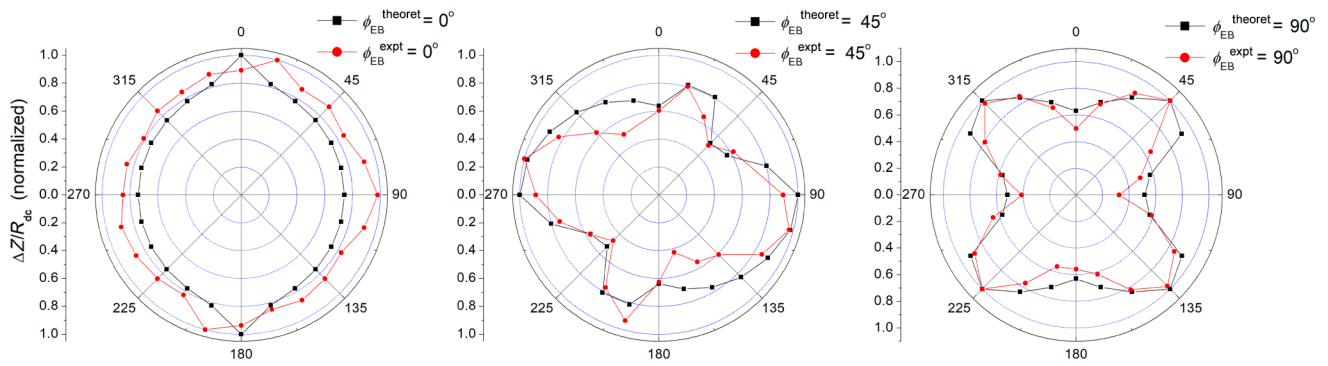
FIG. 6. Normalized impedance ratios versus magnetic field for different angles of the applied magnetic field ($\phi_{EB} = 0°$, $45°$, and $90°$). Theoretical and experimental values are represented by black and red squares, respectively.

For $\phi_{EB} = 45°$ and $\phi_{EB} = 90°$, the MI response is maximized when the external field is oriented midway between the geometrical long axis and H_{EB}, where a maximum in susceptibility occurs and, in consequence, a maximum in the MI magnitude. Therefore, for $\phi_{EB} = 45°$, a maximum of the MI ratio occurs when H_{ext} is applied at angles of $15°$, $105°$, $195°$, and $285°$; for $\phi_{EB} = 90°$ the maximum occurs at angles of $45°$, $135°$, $225°$, and $315°$. When $\phi_{EB} = 0°$, the exchange-bias field is aligned with the geometrical long axis and the maximum MI response occurs at the same angle, $\phi_{ext} = 0°$.

The theoretical model provides excellent agreement with the experimental results as shown for $\phi_{EB} = 0°$, $45°$, and $90°$, where the maximum MI response occurs at $\phi_{ext} \cong 0°$, $15°$, and $45°$, respectively.

In conclusion, these results provide a complete experimental and theoretical description of the MI response in exchange-biased multilayer systems, allowing the control of the asymmetric behavior and magnitude of the MI peaks by tuning the direction of the exchange-bias field, the applied magnetic field, and the probe frequency.

ACKNOWLEDGMENTS

[1] L. V. Panina and K. Mohri, Magnetoimpedance effect in amorphous wires, Appl. Phys. Lett. **65**, 1189 (1994).

[2] R. S. Beach and A. E. Berkowitz, Giant magnetic field dependent impedance of amorphous FeCoSiB wire, Appl. Phys. Lett. **64**, 3652 (1994).

[3] A. Zhukov, J. Gonzalez, J. M. Blanco, M. Vazquez, and V. Larin, Microwires coated by glass: A new family of soft and hard magnetic materials, J. Mater. Res. **15**, 2107 (2000).

[4] B. Hernando, M. L. Sanchez, V. M. Prida, M. Tejedor, and M. Vazquez, Magnetoimpedance effect in amorphous and nanocrystalline ribbons, J. Appl. Phys. **90**, 4783 (2001).

[5] K. Mohri, T. Uchiyama, and L. V. Panina, Recent advances of micro magnetic sensors and sensing application, Sens. Actuators A: Phys. **59**, 1 (1997).

[6] D. Karnaushenko, D. D. Karnaushenko, D. Makarov, S. Baunack, R. Schaefer, and O. G. Schmidt, Self-assembled on-chip-integrated giant magneto-impedance sensorics, Adv. Mater. **27**, 6582 (2015).

[7] L. Kraus, Z. Frait, K. Pirota, and H. Chiriac, Giant magnetoimpedance in glass-covered amorphous microwires, J. Magn. Magn. Mater. **254**, 399 (2003).

[8] C. Gomez-Polo, M. Vazquez, and M. Knobel, Rotational giant magnetoimpedance in soft magnetic wires: Modelization through Fourier harmonic contribution, Appl. Phys. Lett. **78**, 246 (2001).

[9] L. V. Panina, K. Mohri, and D. P. Makhnovskiy, Mechanism of asymmetrical magnetoimpedance in amorphous wires, J. Appl. Phys. **85**, 5444 (1999).

[10] R. B. da Silva, A. D. C. Viegas, V. P. Nascimento, M. A. Correa, L. F. Schelp, E. Baggio-Saitovitch, and R. L. Sommer, High frequency magnetoimpedance in Ni81Fe19/Fe50Mn50 exchange biased multilayer, Appl. Phys. Lett. **94**, 042501 (2009).

[11] C. Garcia, J. M. Florez, P. Vargas, and C. A. Ross, Asymmetrical giant magnetoimpedance in exchange-biased NiFe, Appl. Phys. Lett. **96**, 232501 (2010).

[12] C. Garcia, J. M. Florez, P. Vargas, and C. A. Ross, Effect of the exchange bias coupling strength on the magnetoimpedance of IrMn/NiFe films, J. Appl. Phys. **109**, 07D735 (2011).

[13] R. B. da Silva, M. A. Corra, E. F. Silva, T. J. A. Mori, R. D. Della Pace, R. Dutra, A. D. C. Viegas, F. Bohn, and R. L. Sommer, Angular dependence of asymmetric magnetoimpedance in exchange biased NiFe/IrMn multilayers, Appl. Phys. Lett. **104**, 102405 (2014).

[14] R. da Silva, E. Silva, T. Mori, R. D. Pace, R. Dutra, M. Correa, F. Bohn, and R. Sommer, Improving the sensitivity of asymmetric magnetoimpedance in exchange biased NiFe/IrMn multilayers, J. Magn. Magn. Mater. **394**, 87 (2015).

[15] D. de Cos, N. Fry, I. Orue, L. Panina, A. Garcia-Arribas, and J. Barandiaran, Very large magnetoimpedance (MI) in FeNi/Au multilayer film systems, Sens. Actuators A: Phys. **129**, 256 (2006).

[16] C. Dong, S. Chen, and T. Hsu, A simple model of giant magneto-impedance effect in amorphous thin films, J. Magn. Magn. Mater. **250**, 288 (2002).

[17] C. Dong, S. Chen, and T. Hsu, A modified model of GMI effect in amorphous films with transverse magnetic anisotropy, J. Magn. Magn. Mater. **263**, 78 (2003).

[18] L. Panina and K. Mohri, Effect of magnetic structure on giant magneto-impedance in Co-rich amorphous alloys, J. Magn. Magn. Mater. **157**, 137 (1996).

[19] A. Aharoni, Demagnetizing factors for rectangular ferromagnetic prisms, J. Appl. Phys. **83**, 3432 (1998).

[20] F. Jin, J. Li, L. Zhou, J. Peng, and H. Chen, Simulation of giant magnetic-impedance effect in Co-based amorphous films with demagnetizing field, IEEE Trans. Magn. **51**, 1 (2015).

[21] I. Mayergoyz and G. Bertotti, *The Science of Hysteresis*, 2.c. (Academic Press, Oxford, 2006).

[22] S. Vongtragool, B. Gorshunov, A. A. Mukhin, J. van Slageren, M. Dressel, and A. Müller, High-frequency magnetic spectroscopy on the molecular magnetic cluster V15, Phys. Chem. Chem. Phys. **5**, 2778 (2003).